# Complex Singular Value Decomposition Analysis of Equatorial Waves in the Pacific Observed by TOPEX/Poseidon Altimeter

R. DWI SUSANTO, QUANAN ZHENG, AND XIAO-HAI YAN

*Center for Remote Sensing, Graduate College of Marine Studies, University of Delaware, Newark, Delaware*

(Manuscript received 28 October 1996, in final form 28 July 1997)

ABSTRACT

The mean of the sea level deviation data derived from the TOPEX/Poseidon altimeter in the equatorial Pacific, between 10°S and 10°N, and between 120°E and 78°W, from cycles 2 to 136 (3 October 1992–2 June 1996), are extracted using a maximum–minimum average method. Then, two-dimensional (2D) sea level deviation time series are developed to visualize the dynamics of equatorial waves. The complex singular value decomposition (CSVD) method is applied to decompose these 2D time series into empirical orthogonal modes. Using this method, zonal and meridional structures, propagation directions, periods, and propagation speeds of these empirical modes are obtained.

The first empirical mode is propagating westward, and its structure is asymmetric to the equator. It has an average phase speed $c = -0.6$ m s$^{-1}$ within 4°–6°N and $c = -0.4$ m s$^{-1}$ within 6°–8°S, respectively, and a period of 15 months, which is associated with an interannual Rossby wave. The second empirical mode is propagating eastward along the equator and has a phase speed of 2.5 m s$^{-1}$ and a period of 7 months, which is associated with an equatorial Kelvin wave.

The asymmetric feature of the empirical Rossby wave, which is also observed in the equatorial Pacific, may suggest that the background currents and wind fields in the equatorial Pacific Ocean affect its propagation. The amplitude of the empirical Kelvin mode increases as it propagates eastward. This is associated with an eastward shoaling of the thermocline depth along the equatorial Pacific Ocean. The results of both empirical modes are consistent with those predicted by the theory of Kelvin and Rossby waves and closely represent the actual features of both waves observed in the equatorial Pacific Ocean. Therefore, the CSVD is a suitable method for revealing the dynamics of equatorial waves.

## 1. Introduction

The fundamental theories of equatorially trapped waves have been intensively developed (Moore and Philander 1977; Pedlosky 1987; Philander 1979) and have been verified by in situ observation (Luther 1980; Knox and Halpern 1982; Eriksen et al. 1983). Since the launch of the Seasat altimetry in 1978, the sea level data have been used to investigate the equatorially trapped waves (Malardé et al. 1987). Miller et al. (1988) used the first two years of Geosat (geodetic satellite) sea level data to observe equatorially trapped waves in the Pacific Ocean before and after the 1986–87 El Niño–Southern Oscillation (ENSO) event and found that Kelvin waves propagated across the Pacific with phase speeds of 2.4–2.8 m s$^{-1}$. Delcroix et al. (1991) examined the first year of Geosat sea level data and found evidence of equatorially trapped Kelvin and the first meridional Rossby waves in the Pacific Ocean and gave their phase speeds, estimated by time-lag correlation and least squares fit of the sea level anomaly meridional structures to theoretical modes. White and Tai (1992) used Geosat sea level data to examine the reflection of interannual Rossby waves at the maritime western boundary of the tropical Pacific Ocean and verified the existence of westward-propagating Rossby waves and eastward-propagating Kelvin waves in the equatorial domain. Jacobs et al. (1993) used Geosat data to observe Rossby waves in the whole Pacific Ocean. Zheng et al. (1994) used satellite data to verify the effect of shear flow on the propagation of Rossby waves in the equatorial Pacific, and Zheng et al. (1995) used Geosat sea level data to observe the behavior of the frequency spectra of equatorial waves, especially during the 1986–87 ENSO event. Boulanger and Menkes (1995) used the TOPEX/Poseidon (T/P) sea level data combined with the Tropical Ocean Global Atmosphere–Tropical Atmosphere

*Corresponding author address:* Dr. Xiao-Hai Yan, Center for Remote Sensing, Graduate School of Marine Studies, University of Delaware, Newark, DE 19716-3501.
E-mail: xiao.yan@mvs.udel.edu

Ocean (TOGA–TAO) mooring array to study propagations and reflections of long equatorial waves in the Pacific during the 1992–93 El Niño. Chelton and Schlax (1996) used T/P data to observe global Rossby waves. To distinguish Kelvin and Rossby waves, the previous investigators (e.g., White and Tai 1992; Zheng et al. 1995; Boulanger and Menkes 1995; Boulanger and Fu 1996) decomposed meridional structure of sea level into theoretical Kelvin–Rossby wave modes. This method is widely used; however, it is worth noting that this decomposition does not satisfy the orthogonality relation. Our effort is seeking a new method that is able to decompose a time series into orthogonal modes and is suitable for analyzing 20 distributions of sea level variability observed by satellite altimeters.

A common method to decompose a signal into orthogonal modes is empirical orthogonal functions (EOFs) or principle component analysis; however, this method cannot be used for detection of propagating features because of the lack of phase information. Barnett (1983) applied a complex EOF analysis using a covariance matrix to investigate the interaction of the monsoon and trade wind systems in the Pacific, and he detected propagating features in the wind systems. In this study we use a complex singular value decomposition (CSVD) for which the covariance matrix is not needed, making this method simpler and more efficient. Using CSVD, one can calculate not only the eigenvalues and eigenvectors but also the spatial amplitudes, and spatial and temporal phase functions, from which one can observe the eastward–westward propagation of equatorial waves. Their wavenumbers $k$ and angular velocities $\omega$ can also be derived. Furthermore, the phase speed can be obtained using the dispersion relation $c = \omega/k$.

In this study, our goal is to seek a method to decompose a 2D time series, T/P sea level deviation (SLD) data into orthogonal modes and to reveal the propagation directions, propagation speeds, periods, and zonal and meridional structures of equatorial waves. The following sections of this paper show that the CSVD method does satisfy these requirements. The theory of CSVD is discussed in detail in section 2. Section 3 discusses the application of CSVD to the T/P sea level deviation data in the equatorial Pacific. Section 4 provides a summary.

## 2. Complex singular value decomposition (CSVD)

Before applying the CSVD method to the sea level deviation data, the data have to be transformed into a complex signal using the *Hilbert transform.* The sea level deviation time series $h(t)$ is the real part of a complex function, that is,

$$h(t) = \mathrm{Re}[\psi(t)], \tag{1}$$

where

$$\psi(t) = h(t) + i\xi(t). \tag{2}$$

Then $\xi(t)$ is the Hilbert transform of $h(t)$:

$$\xi(t) = \mathcal{H}[h(t)] = \frac{1}{\pi}\int_{-\infty}^{\infty}\frac{h(u)}{t-u}\,du. \tag{3}$$

The Hilbert transform, therefore, is equivalent to a phase shift of $\pm\pi$ in the spectral domain. In practice, when working with discrete spectra computed using the fast Fourier transform, the determination of $\psi_i$ from $h_i$ is handled most easily by computing the transform of $h(t)$ and then computing the Fourier transform of $\psi(t)$ or $F_\psi$.

The 2D complex sea level deviation time series $\mathbf{h}(x, y, t)$ can be reduced to $\mathbf{D}(x', t)$. Assume $\mathbf{D}$ is an $m$ (spatial points) by $n$ (temporal points) matrix, then

$$\mathbf{D} = \mathbf{USV}^{\mathrm{H}}, \tag{4}$$

where $\mathbf{V}^{\mathrm{H}}$ is the conjugate transpose of $\mathbf{V}$ (Strang 1988). The columns of $\mathbf{U}$ ($m \times m$) are eigenvectors of $\mathbf{DD}^{\mathrm{H}}$, and the columns of $\mathbf{V}$ ($n \times n$) are eigenvectors of $\mathbf{D}^{\mathrm{H}}\mathbf{D}$. The $r$ singular values on the diagonal of $\mathbf{S}$ ($m \times n$) are the square roots of the nonzero eigenvalues of both $\mathbf{DD}^{\mathrm{H}}$ and $\mathbf{D}^{\mathrm{H}}\mathbf{D}$, where $r$ is the rank of $\mathbf{D}$. For complex matrices, $\mathbf{S}$ remains real, $\mathbf{U}$ and $\mathbf{V}$ become *unitary* (the complex analog of orthogonal), which means

$$\mathbf{U}^{\mathrm{H}}\mathbf{U} = \mathbf{I} \quad \text{and}$$
$$\mathbf{V}^{\mathrm{H}}\mathbf{V} = \mathbf{I}. \tag{5}$$

One can see that the columns of $\mathbf{U}$ are eigenvectors of $\mathbf{DD}^{\mathrm{H}}$, and the columns of $\mathbf{V}$ are eigenvectors of $\mathbf{D}^{\mathrm{H}}\mathbf{D}$ using the following expansions:

$$\begin{aligned}\mathbf{DD}^{\mathrm{H}} &= (\mathbf{USV}^{\mathrm{H}})(\mathbf{USV}^{\mathrm{H}})^{\mathrm{H}} = (\mathbf{USV}^{\mathrm{H}}\mathbf{VS}^{\mathrm{T}}\mathbf{U}^{\mathrm{H}})\\ &= \mathbf{USS}^{\mathrm{T}}\mathbf{U}^{\mathrm{H}},\\ \mathbf{D}^{\mathrm{H}}\mathbf{D} &= (\mathbf{USV}^{\mathrm{H}})^{\mathrm{H}}(\mathbf{USV}^{\mathrm{H}}) = (\mathbf{VS}^{\mathrm{T}}\mathbf{U}^{\mathrm{H}}\mathbf{USV}^{\mathrm{H}})\\ &= \mathbf{VS}^{\mathrm{T}}\mathbf{SV}^{\mathrm{H}},\end{aligned} \tag{6}$$

where $\mathbf{S}^{\mathrm{T}}$ is the transpose of $\mathbf{S}$.

To aid in the interpretation, we offer an example, $D(x, t) = a\exp[i(kx - \omega t)]$. Following Barnett (1983), we define the following parameters, which constitute a general description of propagating patterns.

### *a. Spatial amplitude function $S_n(x)$*

The spatial amplitude function shows the spatial distribution of variability associated with each eigenmode and may be interpreted as in a regular EOF or singular valve decomposition (SVD) analysis. To find the amplitude, let the matrix $\mathbf{A}$ satisfy the following relation:

$$\mathbf{D}^{\mathrm{H}} = \mathbf{VA}^{\mathrm{H}}, \tag{7}$$

which, by comparison with Eq. (4), gives $\mathbf{A} = \mathbf{US}$. Then $S_n(x)$ is defined as the real value of complex matrix $\mathbf{A}$, where $n$ represents mode number. For a sinusoid function, $S_n(x)$ is a constant since $a$ is independent of $x$.

*b. Spatial phase function $\theta_n(x)$*

The spatial phase function shows the relative phase of fluctuations among the various spatial locations where **D** is defined. The spatial phase function is defined as

$$\theta_n(x) = \arctan\left(\frac{\mathrm{Im}[A_n(x)]}{\mathrm{Re}[A_n(x)]}\right). \quad (8)$$

The spatial derivative of $\theta_n(x)$ provides, for the sinusoid field, a measure of the local wavenumber $k$.

*c. Temporal amplitude function $R_n(t)$*

Similar to the spatial amplitude function, the temporal amplitude function is defined such that matrix **B** satisfies the following relation:

$$\mathbf{D} = \mathbf{U}\mathbf{B}^{\mathrm{H}}, \quad (9)$$

which, by comparison with Eq. (4), gives $\mathbf{B} = \mathbf{V}\mathbf{S}^{\mathrm{T}}$. Then $R_n(t)$ is defined as the real value of complex matrix **B**. This temporal amplitude function measures the temporal variability in the magnitude of the modal structure of **D**.

*d. Temporal phase function $\phi_n(t)$*

The temporal phase function describes the temporal variation of phase associated with **D**,

$$\phi_n(t) = \arctan\left(\frac{\mathrm{Im}[B_n(t)]}{\mathrm{Re}[B_n(t)]}\right). \quad (10)$$

For the sinusoid wave, one can see that $\phi_n(t) = \omega t$. Therefore, the time derivative of $\phi_n(t)$ is directly proportional to the angular frequency $\omega$.

## 3. Application of CSVD to T/P data in the equatorial Pacific

*a. TOPEX/Poseidon sea level data*

The T/P sea level data are derived from raw T/P data at the National Oceanic and Atmospheric Administration (NOAA) Geoscience Laboratory. The data used in this study have a spatial resolution of 1.0° latitude by 2.8° longitude and cover 60°S–60°N from cycles 2 to 136 (3 October 1992–2 June 1996). Standard corrections have been applied to remove signals from the wet and dry troposphere, ionosphere, tides, inverse barometric pressure, sea state bias, geoid, and orbit errors. Then the sea level time series are expressed as deviations relative to the 3-yr mean: January 1993–96.

The baseline used for this study is a subdataset of the T/P sea level deviation time series, which is taken from the area between 10°S and 10°N and between 120°E and 78°W in the equatorial Pacific Ocean. One can use data from either ascending or descending orbits or both; however, one should note that there are time lags between ascending and descending orbits. To avoid additional bias in the data, we use the data taken from descending orbits only. The original data contain high-frequency signals of which the amplitudes are of the order of 3 cm, which is of the same order of magnitude as the resolution limit of the T/P altimeter. In this study we focus on analyzing the low-frequency variability of sea level regardless of high-frequency components. To extract low-frequency components from the original data, a maximum–minimum mean method (Huang et al. 1998, manuscript submitted to *Proc. Roy. Soc. London, Ser. A*), which is particularly suitable for analyzing nonstationary time series data, is used. A moving average and median filter are also applied to processed data in order to smooth the data further. Figure 1a shows an example of the original SLD data, and Fig. 1b shows the low-frequency variability of the SLD obtained using the above processing techniques. Figure 2 shows time–longitude panels of the low-frequency variability of SLD along the equator, 6°N, and 6°S. Along the equator there are eastward-propagating patterns, which are probably associated with equatorial Kelvin waves; meanwhile along 6°N and 6°S there are westward-propagating patterns that are probably associated with Rossby waves. The solid lines represent the zero value of SLD. Then, 2D time series of low-frequency variability of SLD are

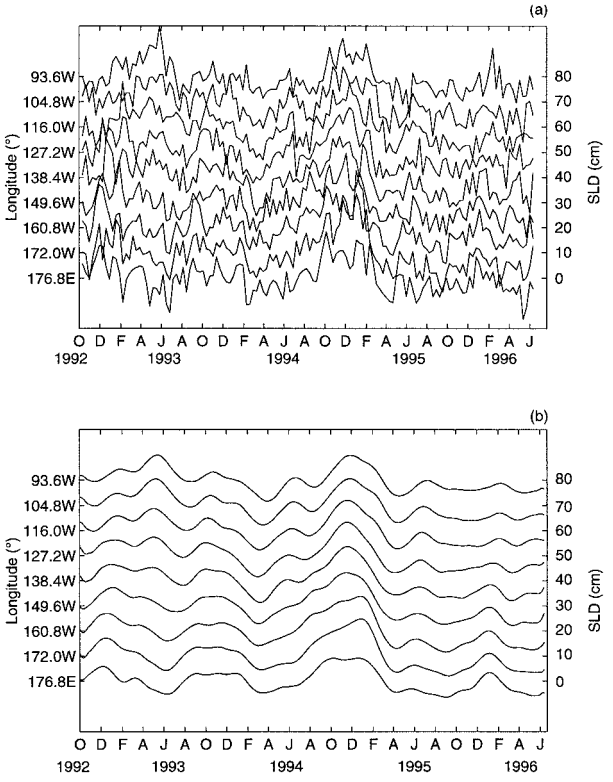


FIG. 1. (a) An example of the original SLD data. (b) The low-frequency variability of SLD after the data processing techniques have been applied.

developed for visualizing the spatial structure and propagation of the equatorial waves (Fig. 3).

### *b. A case study of CSVD analysis*

A subset of 2D sea level deviation time series from March 1993 to January 1994, which is associated with the 1992–93 El Niño event, is analyzed. Figure 3 shows the 2D low-frequency variability of SLD; these are selected as an example of a total of 30 cycles of T/P data during this period. Before May 1993, one can clearly see a Kelvin wave approaching the eastern Pacific and then, about 1 month later, a Rossby wave is observed propagating westward. These figures provide evidence of the reflection of an equatorial Kelvin wave and its transformation into a Rossby wave at the eastern Pacific boundary. One can also see that the meridional structure of the Rossby wave propagating westward is asymmetric to the equator. To reveal more details of these waves, the CSVD method is used to decompose a 2D SLD time series into eastward and westward propagating orthogonal modes. The phase speeds of these modes will also be calculated. We wish to resolve the asymmetric meridional structure of the Rossby wave in the real ocean, as shown in Fig. 3.

Using the CSVD method, we obtain 2D empirical orthogonal modes of 2D SLD time series. Figure 4a shows the first empirical mode, which has a similar structure to that of a theoretical Rossby wave mode, and Fig. 4b shows the second empirical mode, which has a similar structure to that of a theoretical Kelvin wave mode. From Fig. 4a, one can clearly see that the meridional structure of empirical mode 1 is asymmetric to the equator. As mentioned earlier, we have observed an asymmetric structure of the equatorial Rossby wave propagating westward in the 2D time series shown in Fig. 3. In our parallel study (Zheng et al. 1997), we observed that the westerly wind burst, which is most likely responsible for generating equatorial waves, is asymmetric to the equator. This wind causes the asymmetric meridional structure of the Intertropical Convergence Zone (ITCZ) and the thermocline depth, which then force the meridional structure of Rossby waves to be asymmetric to the equator.

From Fig. 4b, one can see that the amplitude of the empirical Kelvin wave increases as it propagates eastward. This result agrees with our results of an equatorial Kelvin solitary wave using the same dataset (Zheng et al. 1998, manuscript submitted to *J. Phys. Oceanogr.*, hereafter referred to as Z98), that is, sea level deviation pulses are consistent with a Kelvin soliton solution of the perturbed KdV equation (PKdV) derived by Long and Chang (1990). In the western Pacific, the thermocline depth is nearly constant at 160-m depth, and it begins shoaling at 175°W up to 60-m depth in the eastern Pacific Ocean. The equilibrium depth of the thermocline changes seasonally. Because of the eastward shoaling of the thermocline depth along the equatorial Pacific, the amplitude of the Kelvin wave increases as it propagates eastward. The effect of the eastward shoaling thermocline depth on the propagation of linear Kelvin waves has been studied by Hughes (1981), who concluded that the amplitude of Kelvin waves increase as they propagate eastward in the equatorial Pacific. This phenomenon is similar to that of a surface gravity wave approaching a shoaling beach. In addition, the nonlinear behavior of equatorial waves has been studied theoretically by Boyd (1980, 1984, 1990) and observed by Glazman et al. (1996).

In order to compare the empirical modes with the theoretical Kelvin–Rossby wave modes, the empirical modes are decomposed into these nonorthogonal modes. Tables 1 and 2 show the relative amplitudes of the first six Kelvin–Rossby wave modes derived from the first and second empirical modes at selected longitudes, respectively. Figures 5a and 5b show a comparison of meridional structures of the first and second empirical modes at selected longitudes with superpositions of those of the first eight theoretical Kelvin–Rossby wave modes. From Table 1, one can see that in the central Pacific, the first empirical mode is primarily composed of the first four Rossby modes and the Kelvin mode. The Rossby mode 2 is the most dominant and the contributions of the Kelvin mode and Rossby modes 1, 3, and 4 are all of the same order of magnitude. Meanwhile, in the eastern Pacific, the meridional structure of this empirical mode is dominated by the first two Rossby modes, where the second mode is more dominant than the first mode. As shown later, these results are also confirmed by the phase speeds. Table 2 shows that the second empirical mode is dominated by the Kelvin mode, which is 3–20 times larger than the first two Rossby modes, depending on the longitude.

After determining the spatial amplitude of the empirical modes, the next step is to calculate their temporal amplitudes. Figures 6a and 6b show the feather plot of the imaginary and the real parts of the temporal amplitude function of the empirical modes 1 and 2, respectively. This function represents temporal variability of the sea level. A semiregular clockwise rotation shown in these figures proves that indeed there is a propagating pattern (if there is no propagating pattern, the vectors or ''sticks'' will be vertical since there is no imaginary part or phase information). For periodic signals, the period of the empirical mode can be obtained from this function directly. However, the length of ours is too short to derive the periods of the waves, and the waves are probably even aperiodic; therefore, the values given here are an approximation only. From Fig. 6a, the period of the first empirical mode is 15 months, which is probably associated with an interannual Rossby wave. Meanwhile, from Fig. 6b, the period of the second empirical mode, associated with a Kelvin wave, is 7 months. As shown later, these periods agree with those derived from the temporal phase functions. The period of Rossby waves can span timescales of several days to several

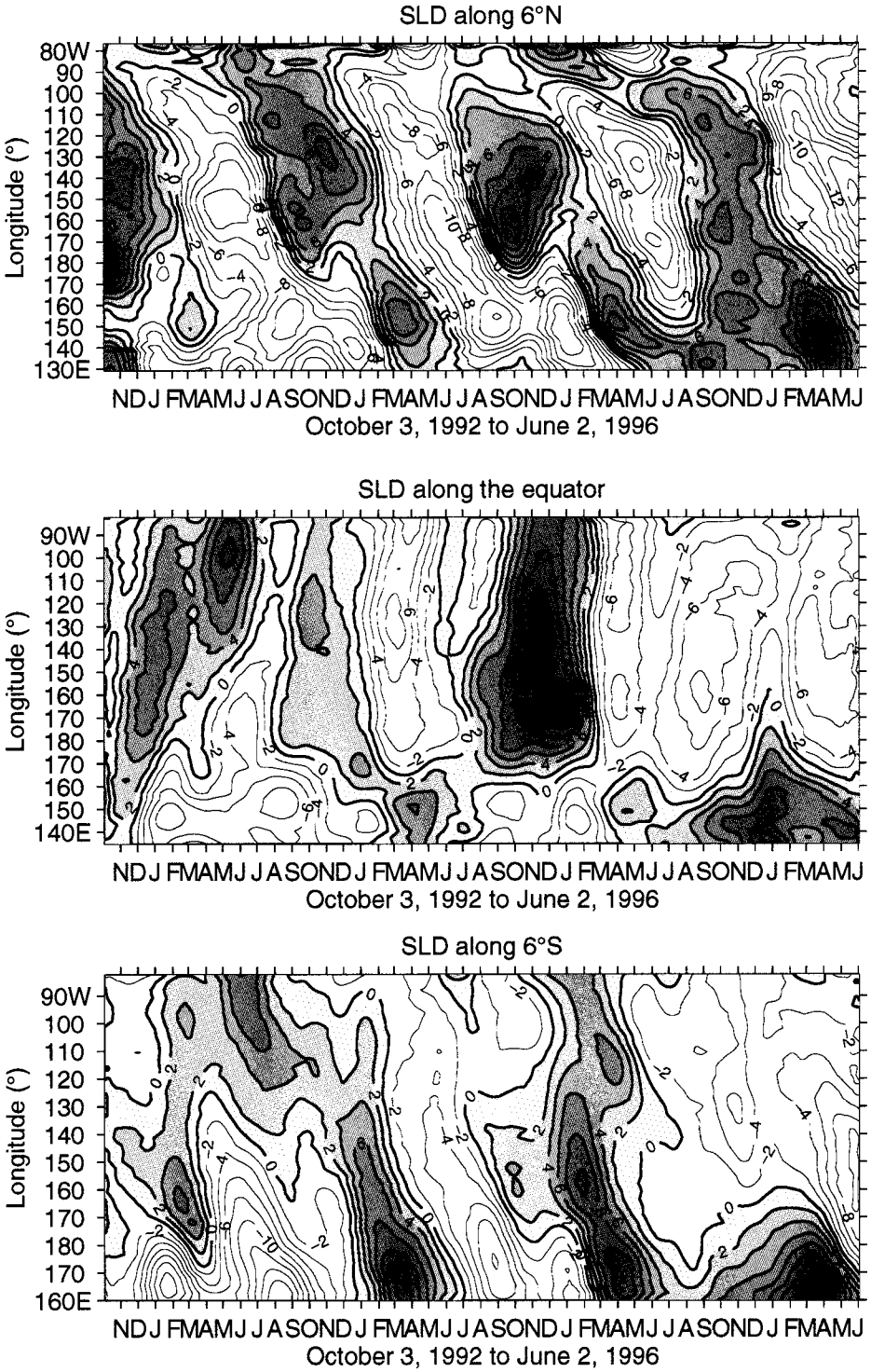


FIG. 2. Time–longitude panels of the low-frequency variability of SLD along the equator, 6°N and 6°S.

years, with length scales ranging from tens of kilometers to several thousand kilometers (Jacobs et al. 1993). The period of the empirical Rossby wave obtained in this study lies within this timescale.

In order to determine the propagation directions of these empirical modes, their spatial phase functions $\theta_n(x)$ and temporal phase functions $\phi_n(t)$ must be calculated. The spatial derivative of $\theta_n(x)$ represents wavenumber $k$, while the temporal derivative of $\phi_n(t)$ represents the angular frequency $\omega$, which is assumed al-

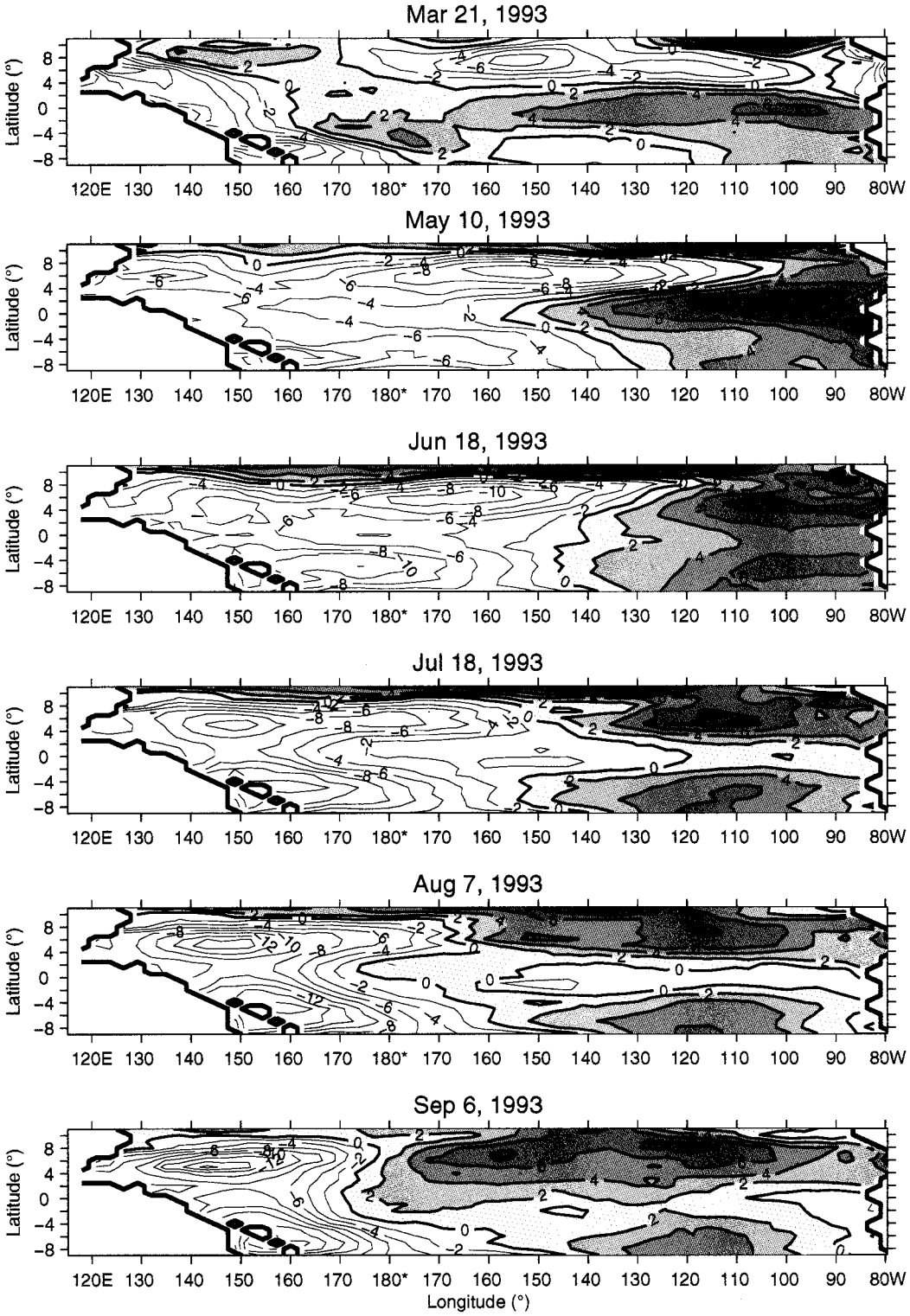


FIG. 3. Two-dimensional low-frequency variability of SLD time series; these are selected as an example of a total of 30 cycles of TOPEX/Poseidon data from March 1993 to January 1994.

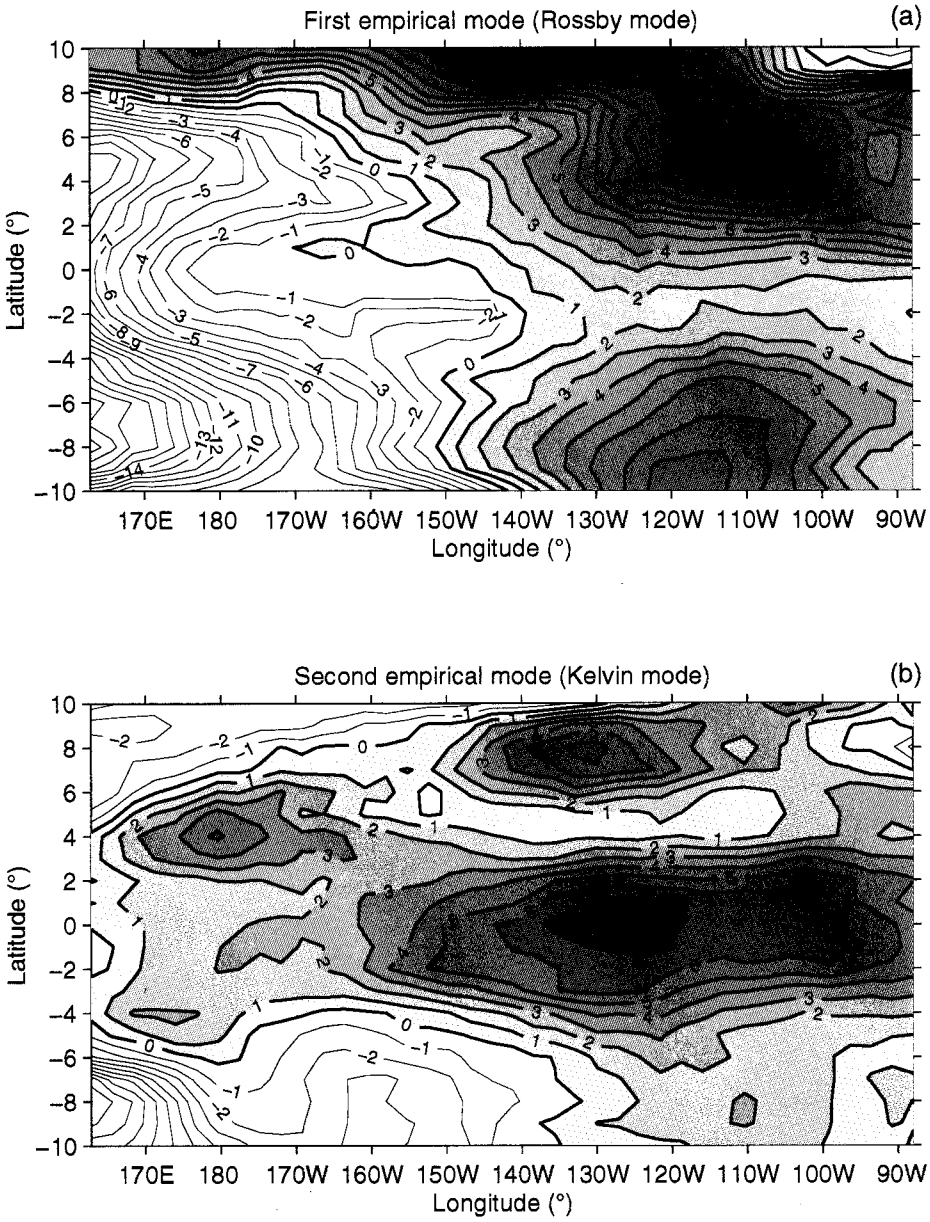


FIG. 4. The spatial amplitudes of (a) the first empirical mode and (b) the second empirical modes obtained using the CSVD method.

ways to be positive. If the wavenumber $k$ for a given mode is positive, it means that this mode propagates eastward. Otherwise, the mode propagates westward. From Fig. 4, one can see that the peak positions of the empirical Rossby mode are at 4°–6°N and 6°–8°S at the eastern and central Pacific Ocean, respectively. Therefore, the spatial phase functions for both modes are calculated along these latitudes. The results of the first empirical mode are shown in Figs. 7a and 7b, respectively. Figure 7c shows the spatial phase function of the second empirical mode along the equator (1°S–1°N). The symbols are derived from satellite observations, and the solid lines are their linear fits calculated by regressions.

Figures 7d and 7e show the temporal phase functions of the first and second empirical modes, respectively. The dots are derived from satellite observations, and the solid lines are their linear fits calculated by regressions. The slope of the spatial phase function represents the wavenumber, while that for the temporal phase function represents the angular frequency. The first empirical mode has wavenumber $k = -0.029$ rad (°longitude)$^{-1}$ and $k = -0.043$ rad (°longitude)$^{-1}$ within 4°–6°N and 6°–8°S, respectively. The angular frequency of the first

TABLE 1. The empirical Rossby mode decomposed into theoretical Kelvin–Rossby wave modes at selected longitudes: *K* is the theoretical Kelvin wave mode and $R - n$ is the theoretical Rossby wave mode *n*, where *n* is mode number.

| | Relative amplitude | | | | | |
|---|---|---|---|---|---|---|
| Long | K | $R-1$ | $R-2$ | $R-3$ | $R-4$ | $R-5$ |
| 165.6°E | −16.63 | −12.70 | −47.96 | 12.97 | −10.98 | 3.00 |
| 168.4°E | −17.12 | −12.71 | −38.72 | 12.07 | −11.28 | 2.95 |
| 171.2°E | −10.73 | −13.39 | −32.68 | 12.51 | −11.00 | 2.95 |
| 174.0°E | −2.50 | −10.49 | −29.29 | 10.82 | −10.52 | 2.93 |
| 176.8°E | 8.00 | −9.84 | −29.44 | 10.01 | −8.77 | 2.86 |
| 124.4°W | −3.26 | 27.79 | 34.91 | 2.99 | 6.17 | 0.30 |
| 118.8°W | −7.46 | 33.09 | 38.54 | 1.92 | 7.34 | 0.16 |
| 113.2°W | −17.48 | 25.87 | 45.73 | 3.91 | 6.11 | −0.60 |
| 107.6°W | −15.40 | 24.94 | 43.24 | 4.69 | 5.31 | −1.21 |
| 102.0°W | −7.86 | 31.19 | 36.47 | 2.29 | 5.86 | −0.42 |

TABLE 2. The empirical Kelvin mode decomposed into theoretical Kelvin–Rossby wave modes at selected longitudes: *K* is the theoretical Kelvin wave mode and $R - n$ is the theoretical Rossby wave mode *n*, where *n* is mode number.

| | Relative amplitude | | | | | |
|---|---|---|---|---|---|---|
| Long | K | $R-1$ | $R-2$ | $R-3$ | $R-4$ | $R-5$ |
| 169.2°W | 14.38 | −3.47 | 4.43 | 6.34 | −1.84 | −0.46 |
| 163.6°W | 22.97 | −1.72 | 1.22 | 6.41 | −2.35 | 0.02 |
| 158.0°W | 36.76 | −1.86 | −2.17 | 4.25 | −2.26 | 0.60 |
| 152.4°W | 46.38 | −14.31 | −1.54 | 4.80 | −1.94 | 0.23 |
| 146.8°W | 44.33 | −15.83 | 6.54 | 3.22 | −1.39 | 0.23 |
| 141.2°W | 44.75 | −10.93 | 8.73 | 0.34 | −1.72 | 0.99 |
| 135.6°W | 58.41 | 4.97 | 6.72 | −5.33 | −0.95 | 2.07 |
| 127.2°W | 62.36 | 10.52 | 7.79 | −7.24 | −0.01 | 2.20 |
| 121.6°W | 71.36 | 7.15 | 3.24 | −6.25 | 1.40 | 1.53 |
| 116.0°W | 70.69 | 5.93 | −1.28 | −5.02 | 1.24 | 1.06 |
| 110.4°W | 73.76 | 3.04 | −3.80 | −3.42 | 0.98 | 0.51 |
| 104.8°W | 75.57 | 4.13 | −4.86 | −1.79 | 1.32 | 0.34 |
| 99.2°W | 50.34 | −3.40 | 9.00 | 0.83 | −0.86 | 0.09 |
| 96.4°W | 49.47 | −2.65 | 9.04 | 0.73 | −0.02 | 0.36 |
| 90.8°W | 44.41 | −1.94 | 6.29 | −0.11 | 0.11 | 0.31 |
| 88.0°W | 37.32 | −1.07 | 7.05 | −0.10 | 0.20 | 0.36 |

mode $\omega = 0.014$ rad day$^{-1}$. The second empirical mode has wavenumber $k = 0.016$ rad (°longitude)$^{-1}$ and $\omega = 0.031$ rad day$^{-1}$. From values of wavenumber and angular frequency, one can obtain the periods and wavelengths of these modes. The periods are 15 months and 7 months for the first and the second empirical modes, respectively.

Using the relation $c = \omega/k$, we obtain the average phase speed of the first empirical mode as $-0.6$ m s$^{-1}$ along 4°–6°N, and $-0.4$ m s$^{-1}$ along 6°–8°S associated with a westward-propagating Rossby wave. The average phase speed of the second mode is 2.5 m s$^{-1}$ associated with an eastward-propagating Kelvin wave. There is a difference in the phase speed of Rossby wave within 4°–6°N and that within 6°–8°S, which suggests that the asymmetric peaks of Rossby wave do not propagate westward with a constant speed. This is probably due to the interaction between the waves and background currents in the equatorial Pacific Ocean.

Using the empirical Kelvin wave phase speed (2.5 m s$^{-1}$) and the mean of the empirical Rossby mode phase speed ($-0.5$ m s$^{-1}$), and then applying to the dispersion relation $c_m = c/(1 + 2m)$, where *m* is the Rossby mode number, *c* is the equatorial Kelvin wave speed, and $c_m$ is phase speed of Rossby wave mode *m*, shows that Rossby mode 2 is the most dominant component. This result is confirmed by the mode decompositions into the theoretical Kelvin–Rossby wave modes (see Table 1). The phase speeds of both empirical modes are in good agreement with those predicted by the linear theory of Kelvin and Rossby waves reported by previous investigators (e.g., Luther 1980; Knox and Halpern 1982; Gill 1982; Eriksen et al. 1983; Miller 1988; Delcroix et al. 1991; Zheng et al. 1995; Chelton and Schlax 1996), who predicted that a Kelvin wave phase speed is in the range 2.4–3.1 m s$^{-1}$.

## 4. Summary

The CSVD analysis of the TOPEX/Poseidon sea level deviation data from March 1993 to January 1994 has provided valuable information about the spatial structure in both zonal and meridional directions, propagation directions, periods, and phase speeds of equatorial waves. The first empirical mode is asymmetric to the equator, which is probably due to the wind fields, me-

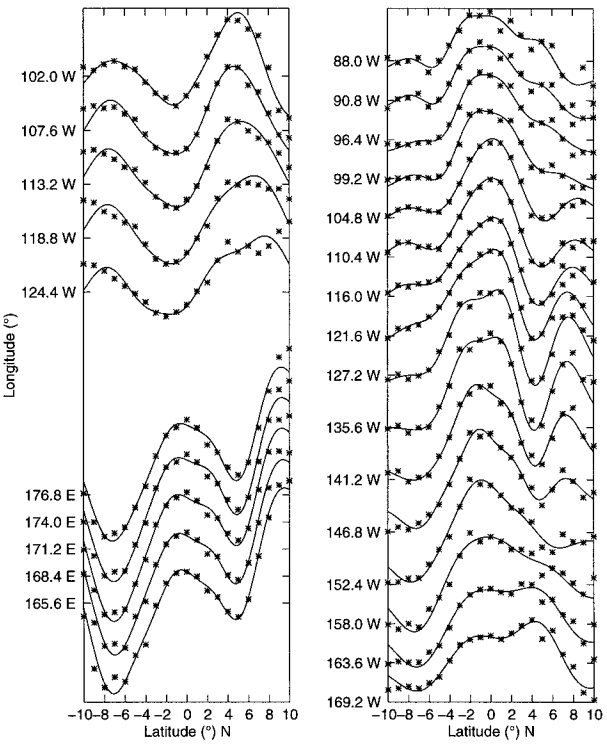


FIG. 5. Comparison of meridional structure of (a) the first and (b) the second empirical modes at selected longitudes with that of theoretical Kelvin–Rossby wave modes. The asterisks represent the empirical modes derived using the CSVD method, while the solid lines are superpositions of the first eight Kelvin–Rossby wave modes.

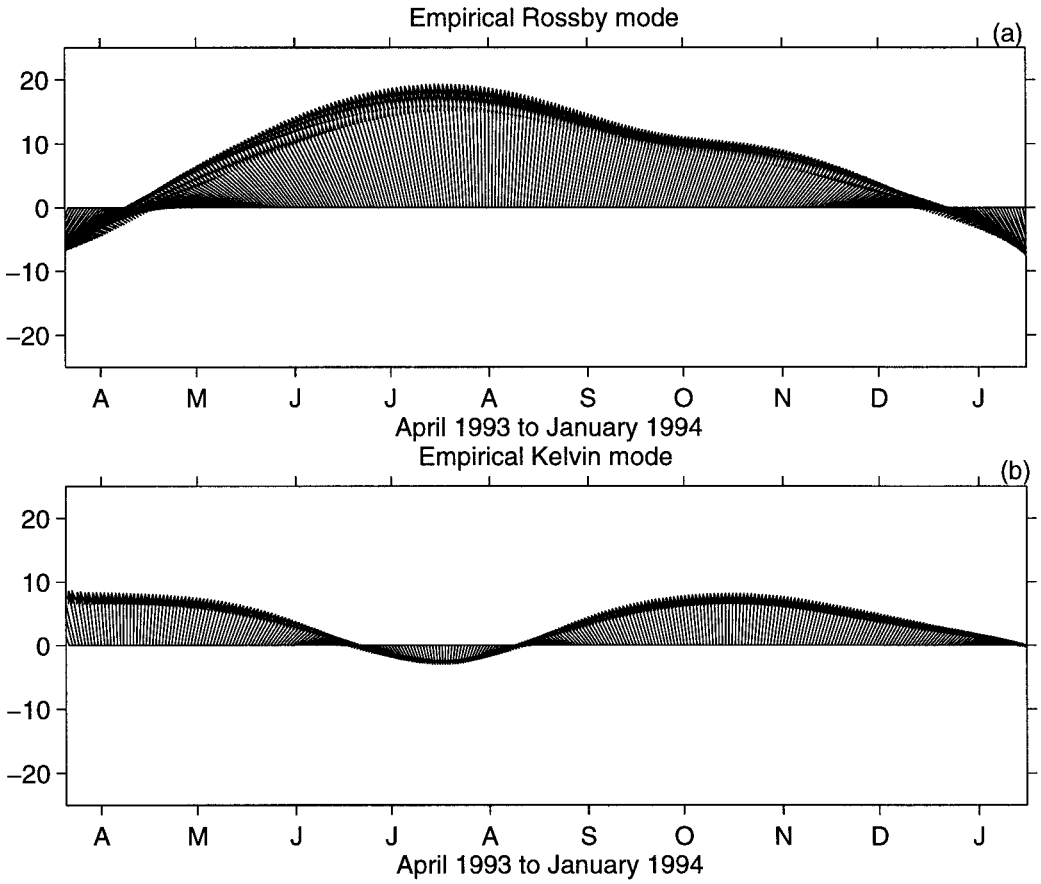


FIG. 6. The feather plot of the imaginary and the real parts of the temporal amplitude functions of (a) the first empirical mode and (b) the second empirical mode.

ridional thermocline depth, and background current effects, and has a similar structure to that of the Rossby wave observed in the real ocean. The second empirical mode structure agrees with that of a Kelvin wave. The amplitude of the second mode increases as it propagates eastward due to the eastward shoaling of the thermocline depth along the equatorial Pacific, as shown in our parallel study of an equatorial Kelvin soliton (Z98) and by previous investigators (Hughes 1981; Long and Chang 1990). In the eastern Pacific, the meridional structure of the first empirical mode is composed mostly of a superposition of the first two theoretical Rossby modes, where the second mode is more dominant than the first. In the central Pacific, this mode is also composed primarily of the second Rossby mode; however, the contributions of the theoretical Kelvin mode and the theoretical Rossby modes 1, 3, and 4 are all of the same order of magnitude. These results are confirmed by their phase speeds. The meridional structure of the second empirical mode agrees well with that of the theoretical Kelvin wave. Based on their temporal modes and temporal phase functions, the period of the first empirical mode is 15 months, which is probably associated with an interannual Rossby wave. The period of the second empirical mode, which is probably associated with a Kelvin wave, is 7 months.

The phase speed of the first mode associated with an interannual Rossby wave is $-0.6$ and $-0.4$ m s$^{-1}$ within the peak at 4°–6°N and 6°–8°S, respectively. This difference is probably due to the influence of background currents in the equatorial Pacific Ocean. The mean of the empirical Rossby mode phase speeds is $-0.5$ m s$^{-1}$. The phase speed of the second mode is 2.5 m s$^{-1}$. Equating these phase speeds to the dispersion relation $c/(1 + 2m)$, where $m$ is the theoretical Rossby mode number and $c$ is the theoretical Kelvin wave speed, shows that Rossby mode 2 is the most dominant component. The mode decompositions of the empirical modes into theoretical Kelvin–Rossby wave modes given in Table 1 confirms this result.

Using the CSVD method we obtain zonal and meridional structures, propagation directions, periods, and propagation speeds of both empirical Kelvin and Rossby waves, where the results are in good agreement with those predicted by the theory of equatorial Kelvin and Rossby waves. The asymmetric feature of the empirical

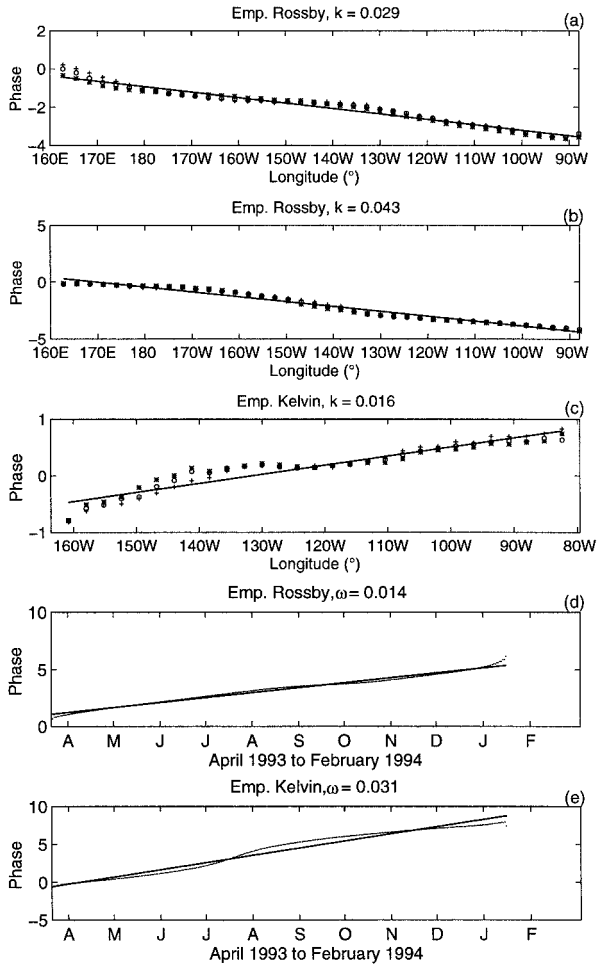


FIG. 7. The spatial phase functions of (a) the first empirical mode along the peak at 4°–6°N, (b) the first empirical mode along the peak at 6°–8°S, and (c) the second empirical mode along the equator (1°S–1°N). Also shown are the temporal phase functions of (d) the first empirical mode and (e) the second empirical mode. The symbols and dots are derived from satellite observation, and the solid lines are their linear fits or slopes calculated by regression.

Rossby mode and the increasing amplitude of the empirical Kelvin mode as it propagates eastward represent the natural features observed in the equatorial Pacific Ocean. Therefore, we believe that this method is a suitable technique for analyzing equatorial wave dynamics.

*Acknowledgments.* This study is partially supported by the National Science Foundation through Grant NSF OCE-9453499 and by the National Aeronautics and Space Administration TOPEX/Poseidon Altimetry Program (Application for Studies of Ocean Dynamics) through Grant NAGW-4771. The author would like to thank Robert Cheney, NOAA/Geoscience Laboratory for providing the T/P data. We would like to thank both anonymous reviewers for their fruitful comments, James Kirby for his helpful discussions, and Simon Shaw and Louis Keiner for preparing the paper.

## REFERENCES

Barnett, T. P., 1983: Interaction of the monsoon and Pacific trade wind systems at interannual time scale. Part I: The equatorial zone. *Mon. Wea. Rev.*, **111,** 756–773.

Boulanger, J.-P., and C. Menkes, 1995: Propagation and reflection of long equatorial waves in the Pacific ocean during the 1992–1993 El Niño. *J. Geophys. Res.*, **100,** 25 041–25 059.

——, and L.-L. Fu, 1996: Evidence of boundary reflection of Kelvin and first-mode Rossby waves from TOPEX/Poseidon sea level data. *J. Geophys. Res.*, **101,** 16 361–16 371.

Boyd, J. P., 1980: Equatorial solitary waves. Part I: Rossby solitons. *J. Phys. Oceanogr.*, **10,** 1699–1717.

——, 1984: Equatorial solitary waves, Part 4: Kelvin solitons in a shear flow. *Dyn. Atmos. Oceans,* **8,** 173–184.

——, 1990: Nonlinear equatorial waves. *Nonlinear Topics in Ocean Physics,* A. R. Osborne and L. Bergamosco, Eds., North-Holland, 51–97.

Chelton, D. B, and M. G. Schlax, 1996: Global observations of oceanic Rossby waves. *Science,* **172,** 234–238.

Delcroix, T., J. Picaut, and G. Eldin, 1991: Equatorial Kelvin and Rossby waves evidenced through Geosat sea level and surface current anomalies. *J. Geophys. Res.,* **96** (Suppl.), 3249–3262.

Eriksen, C. C., M. G. Blumenthal, S. P. Hayes, and P. Ripa, 1983: Wind-generated equatorial Kelvin waves observed across the Pacific Ocean. *J. Phys. Oceanogr.*, **13,** 1622–1640.

Gill, A. E., 1982: *Atmosphere Ocean Dynamics.* Academic Press, 429–491.

Glazman, R. E., A. Frabrikant, and A. M. Greysukh, 1996: Nonlinear features of equatorial baroclinic Rossby waves detected in TOPEX altimeter observations. *Nonlinear Processes Geophys.,* **3,** 115–126.

Hughes, R. L., 1981: The influence of thermocline slope on equatorial thermocline displacement. *Dyn. Atmos. Oceans,* **5,** 147–157.

Jacobs, G. A., W. J. Emery, and G. H. Born, 1993: Rossby waves in the Pacific Ocean extracted from Geosat altimeter data. *J. Phys. Oceanogr.,* **23,** 1155–1175.

Knox, R. A., and D. Halpern, 1982: Long-range wave propagation of transport variation in Pacific Ocean equatorial currents. *J. Mar. Res.*, **40** (Suppl.), 329–339.

Long, B., and P. Chang, 1990: Propagation of an equatorial Kelvin wave in varying thermocline. *J. Phys. Oceanogr.,* **20,** 1826–1841.

Luther, D. S., 1980: Observations of long period waves in the tropical ocean and atmosphere. Ph.D. dissertation, MIT–Woods Hole Oceanographic Institution Joint Program in Oceanography, 209 pp.

Malardé, J.-P., P. deMey, C. Périgaud, and J.-F. Minster, 1987: Observation of long equatorial waves in the Pacific Ocean by Seasat altimetry. *J. Phys. Oceanogr.,* **17,** 2273–2279.

Miller, L., R. E. Cheney, and B. C. Douglas, 1988: GEOSAT altimeter observations of Kelvin waves and the 1986–87 El Niño. *Science*, **239,** 52–54.

Moore, D. W., and S. G. H. Philander, 1977: Modeling of the tropical oceanic circulation. *The Sea,* E. D. Goldberg et al., Eds., Wiley-Interscience, Vol. 6, 319–361.

Pedlosky, J., 1987: *Geophysical Fluid Dynamics.* 2d ed. Springer–Verlag, 710 pp.

Philander, S. G. H., 1979: Equatorial waves in the presence of the equatorial under-current. *J. Phys. Oceanogr.*, **9,** 254–262.

Strang, G., 1988: *Linear Algebra and Its Applications.* 3d ed. Harcourt Brace Jovanovich, 442–451.

White, W. B., and C.-K. Tai, 1992: Reflection of interannual Rossby

waves at the maritime western boundary of the tropical Pacific. *J. Geophys. Res.,* **97,** 14 305–14 322.

Zheng, Q., X.–H. Yan, C.-R. Ho, and C.-K. Tai, 1994: The effects of shear flow on propagation of Rossby waves in the equatorial oceans. *J. Phys. Oceanogr.,* **24,** 1680–1686.

——, ——, ——, and ——, 1995: Observation of equatorially trapped waves in the Pacific using Geosat altimeter data. *Deep-Sea Res.,* **42,** 797–817.

——, ——, W. T. Liu, W. Tang, and D. Kurz, 1997: Seasonal and interannual variability of atmospheric convergence zones in the tropical Pacific observed with *ERS-1* scatterometer. *Geophys. Res. Lett.,* **24,** 261–263.